ISSN: 1687-1006 p
ISSN: 2682-3640 e

The Egyptian International Journal of Engineering Sciences and Technology

https://eijest.journals.ekb.eg/

Vol. 51 (2025) 53–63

DOI: 10.21608/eijest.2024.334181.1304

A Novel Model-Free Continuous Sliding Mode Controller with a PI Sliding Surface for Industrial Robots: Achieving Near-Zero Tracking Errors and GUUB Stability

Khaled R. Atia*

Department of Mechanical Design and Production Engineering, Faculty of Engineering, Zagazig University, Zagazig, 44519, Egypt.

ARTICLE INFO

Article history:

Received 06 November 2024
Received in revised form 08 December 2024
Accepted 08 December 2024
Available online 08 December2024

Keywords:

Robot Control
Sliding Mode Control
Sliding Surface
Boundary Layer
Ultimate Bound.

ABSTRACT

This study presents a novel continuous sliding mode control (SMC) law for robotic arms, emphasizing computational efficiency, structural simplicity, and stability. The proposed controller, which does not require the robot's dynamic model in its structure, ensures Global Uniform Ultimate Bounded (GUUB) stability, focusing on minimizing joint tracking errors. To enhance tracking performance, the control law incorporates a nonlinear function that increases control effort only within the boundary layer, effectively reducing the ultimate bounds of tracking errors. Stability is demonstrated using Lyapunov theory, confirming the asymptotic convergence of tracking errors to near zero. Further improvement is achieved by replacing the original sliding surface with a proportional-integral (PI) sliding surface. This PI-based sliding mode controller maintains GUUB stability while delivering superior tracking accuracy, as evidenced by near-zero ultimate bounds of tracking errors. Simulation results with a two degrees of freedom manipulator validate the controllers' effectiveness in handling disturbances, with the enhanced PI-based controller showing superior performance, nearly eliminating tracking errors.

1. Introduction

Achieving precise, dexterous motion in industrial robot manipulators requires controllers that are robust against external disturbances, unknown payloads, and modelling inaccuracies. Sliding Mode Control (SMC) has emerged as a leading method to address these challenges due to its ability to maintain system performance despite disturbances once the system reaches the sliding mode [1-7]. This is possible because SMC introduces dynamic invariance, making it resilient to disturbances. However, SMC assumes that input control signals can switch instantaneously between different values, which is unattainable in real systems. Physical limitations of actuators and finite computational time delays prevent this instantaneous switching, resulting in a phenomenon known as chattering (high frequency oscillations around the desired equilibrium state) [8-9]. Chattering can excite the unmodeled high-frequency dynamics, degrading the performance of systems.

A common method to remove chattering involves introducing a boundary layer around the sliding manifold, where a continuous control signal replaces the discontinuous one once the system's trajectories enter this layer [10]. While effective in removing

* Corresponding author. Tel.: +002-01224442910; fax: +002-0552304987
E-mail address: k_atia@zu.edu.eg; k_atia@hotmail.com

chattering, this approach of control causes bounded steady-state tracking errors and compromises the system's robustness, which becomes dependent on the width of the boundary layer area.

To address these limitations, various adaptive methods have been proposed. For instance, adjusting the width of the boundary layer zone according to the degree of system uncertainty [11] or using higher-order sliding modes [12] can remove chattering while maintaining tracking accuracy. However, these methods often rely on higher-order derivatives of system states, which may be unmeasurable in practical systems. Other approaches include the use of a low-pass filter between the controller and the plant [13], parameter estimation techniques [14], adaptive control schemes [15-17] and improved reaching laws and sliding surfaces [18]. In addition to the latter methods, continuous sliding mode control of robotic manipulators based on time-varying disturbance estimation and compensation is used to address the high-precision trajectory tracking task of uncertain robot arms [19]. These methods, while effective, always introduce increased complexity and require knowledge of the robot's dynamics, which limits their applicability.

In response to these challenges, this work introduces a novel sliding mode controller (SMC) for rigid robot manipulators that offers a simplified structure without compromising high tracking performance. By leveraging its streamlined design, the proposed control law enhances robustness, simplicity, and computational efficiency compared to advanced controllers, such as traditional sliding mode controllers or adaptive controllers, which typically depend on detailed dynamic models for their implementation.

A key innovation of this controller is the incorporation of a new method to improve control performance within the boundary layer. Unlike conventional approaches, this method does not require explicit knowledge of the robot's dynamic model, thereby reducing complexity and mitigating modeling errors. Furthermore, the controller addresses the chattering phenomenon commonly associated with sliding mode control by ensuring smoother control actions while maintaining robust disturbance rejection and trajectory tracking capabilities.

This generalizable framework extends beyond robotic manipulators and can be adapted to various sliding mode control applications. Its ability to achieve high-precision trajectory tracking under model uncertainties and external disturbances makes it a robust and efficient solution for complex and dynamic systems requiring precise control.

Throughout this research article, bold uppercase letters denote matrices, while vectors are represented by symbols or as defined in the text. The smallest and largest eigenvalues of a symmetric, positive definite, bounded matrix $\mathbf{Q}(\Omega)$ are represented by $\lambda_m\{\mathbf{Q}(\Omega)\}$ and $\lambda_M\{\mathbf{Q}(\Omega)\}$, respectively, for all $\Omega \in \mathbb{R}^n$. The Euclidean norm of any real vector Ω is indicated by $\|\Omega\|$, real numbers are denoted by $\mathbb{R}$, and the identity matrix is represented by $\mathbf{I} \in \mathbb{R}^{n\times n}$.

2. Robot Dynamics and Their Key Properties

If disturbances are considered, the dynamic model of any n-link rigid arm with revolute joints is defined by [20]:

$$\mathbf{H}(\Theta)\ddot{\Theta} + \mathbf{C}(\Theta,\dot{\Theta})\dot{\Theta} + \chi(\Theta) + \tau_d = \tau \qquad (1)$$

where:

- $\Theta \in \mathbb{R}^n$ is the vector of joint positions,
- $\mathbf{H}(\Theta) \in \mathbb{R}^{n\times n}$ is the matrix of inertia which is symmetric and positive definite,
- $\mathbf{C}(\Theta,\dot{\Theta})\dot{\Theta} \in \mathbb{R}^n$ represents the centrifugal and Coriolis force vector,
- $\chi(\Theta) \in \mathbb{R}^n$ is the gravitational force vector,
- $\tau \in \mathbb{R}^n$ is the vector of input torque**,** and
- $\tau_d \in \mathbb{R}^n$ represents the vector of external disturbances, assumed to be bounded by $\|\tau_d\| \le d$, where d is a positive constant [20][21].

This dynamic model possesses the following key properties [20] [22][23]:

P1. The matrix of inertia is a symmetric positive definite bounded matrix.

$$\lambda_m\{\mathbf{H}\}\|\dot{\Theta}\|^2 \le \dot{\Theta}^T\mathbf{H}(\Theta)\dot{\Theta} \le \lambda_M\{\mathbf{H}\}\|\dot{\Theta}\|^2$$

P2. There is a bounded positive constant k_c that satisfies the following inequality:

$$\|\mathbf{C}(z,x)y\| \le k_c\|x\|\|y\| \quad \forall\, x,y,z \in \mathbb{R}^n$$

P3. The matrix $\mathbf{C}(\cdot)$ satisfies commutativity.

$$\mathbf{C}(z,x)y = \mathbf{C}(z,y)x \quad \forall\, x,y,z \in \mathbb{R}^n$$

P4. The matrix $\left(\dot{\mathbf{H}}(\Theta) - 2\mathbf{C}(\Theta,\dot{\Theta})\dot{\Theta}\right)$ is skew-symmetric. This implies:

$$x^T\left\{\dot{\mathbf{H}}(\Theta) - 2\mathbf{C}(\Theta,\dot{\Theta})\dot{\Theta}\right\}x = 0 \quad \forall\, x \in \mathbb{R}^n$$

$$\dot{\mathbf{H}}(\Theta) = \mathbf{C}(\Theta,\dot{\Theta}) + \left\{\mathbf{C}(\Theta,\dot{\Theta})\right\}^T$$

P5. There is a bounded positive constant k_v that satisfies:

$$\|\chi(\Theta)\| \leq k_v \quad \forall\, \Theta \in \mathbb{R}^n$$

3. Preliminary Framework for Controller Design

As an initial step, the proposed continuous sliding mode control law and the associated sliding surface, denoted by $\Gamma \in \mathbb{R}^n$, are defined as follows:

$$\tau = (\alpha\|\Gamma\| + \gamma)\,\mathrm{Sat}(\Gamma) \tag{2}$$

$$\Gamma = \dot{\tilde{\Theta}} + \lambda\,\mathrm{Tanh}(\tilde{\Theta}) \tag{3}$$

Here, $\tilde{\Theta} = \Theta_\mathrm{d} - \Theta$, represents the position error vector, where $\Theta_\mathrm{d} \in \mathbb{R}^n$ is the desired position vector. Additionally, for any $\mathrm{z} \in \mathbb{R}^n$, $\mathrm{Tanh}(\mathrm{z})$ and $\mathrm{Sat}(\mathrm{z})$ are vector functions of dimension n, with elements $\tanh(z_i)$ and $\mathrm{sat}(z_i)$, respectively. The parameters $\alpha, \gamma, \lambda \in \mathbb{R}$ are positive constant gains. For all $\mathrm{z} \in \mathbb{R}^n$, the $\mathrm{Sat}(\mathrm{z})$ vector function is defined as:

$$\mathrm{Sat}(\mathrm{z}) = \begin{cases} \delta^{-1}\,\mathrm{z} & \text{if } \|\mathrm{z}\| \leq \delta \\ \mathrm{Sgn}(\mathrm{z}) & \text{otherwise} \end{cases} \tag{4}$$

Here, $\mathrm{Sgn}(\cdot)$ is the signinum vector function, and δ is a small constant ($\delta < 1$) that defines the well-known boundary layer thickness. The $\mathrm{Tanh}(\cdot)$ vector function satisfies [24]:

$$\tanh(\|\mathrm{z}\|) \leq \|\mathrm{Tanh}(\mathrm{z})\| \leq \begin{cases} \|\,\mathrm{z}\,\| & \forall\ \mathrm{z} \in \mathbb{R}^n \\ \sqrt{n} & \forall\ \mathrm{z} \in \mathbb{R}^n \end{cases} \tag{5}$$

The objective of the above control law is to make the tracking variable Γ reaches zero as quickly as possible. Once this occurs, the differential equation (D.E.) defining Γ reduces to a homogeneous (unforced) differential equation, where its left-hand side equals zero. Since this equation is stable, the tracking error $\tilde{\Theta}$ asymptotically approaches zero. To demonstrate this, consider the Lyapunov function: $V = 0.5\,\tilde{\Theta}^\mathrm{T}\tilde{\Theta}$. The time derivative of this Lyapunov function candidate along the trajectories of the system defined by $\Gamma = 0$ is given by: $\dot{V} = -\lambda\,\tilde{\Theta}^\mathrm{T}\,\mathrm{Tanh}(\tilde{\Theta})$. The structures of V and $\dot{V}$ confirm the asymptotic convergence of $\tilde{\Theta}$ to zero.

3.1 Stability analysis of the preliminary controller

Consider the following Lyapunov function:

$$V_1 = 0.5\,\Gamma^\mathrm{T}\mathbf{H}(\Theta)\Gamma \tag{6}$$

Using property P1, we obtain:

$$0.5\,\lambda_m\{\mathbf{H}\}\,\|\Gamma\|^2 \leq V_1 \leq 0.5\,\lambda_M\{\mathbf{H}\}\,\|\Gamma\|^2 \tag{7}$$

The time derivative of the function V_1 along the trajectories of the system defined by Eqs. (1) and (2) is given by:

$$\dot{V}_1 = \frac{1}{2}\Gamma^\mathrm{T}\dot{\mathbf{H}}(\Theta)\Gamma + \Gamma^\mathrm{T}\Big\{\mathbf{C}(\Theta,\dot{\Theta})\dot{\Theta} + \chi(\Theta) - \tau + \mathbf{H}(\Theta)\ddot{\Theta}_\mathrm{d} + \mathbf{H}(\Theta)\,\mathbf{A}(\tilde{\Theta})\dot{\tilde{\Theta}} + \tau_\mathrm{d}\Big\} \tag{8}$$

Here, $\mathbf{A}(\tilde{\Theta}) \leq \mathbf{I}\ \forall\ \tilde{\Theta} \in \mathbb{R}^n$ is a diagonal matrix defined by $\mathbf{A}_{ii} = \left(\mathrm{sech}(\tilde{\theta}_i)\right)^2\ \forall i = 1{:}\,n$.

By using property P3 along with the definition of Γ, we obtain:

$$\mathbf{C}(\Theta,\dot{\Theta})\dot{\Theta} = -\mathbf{C}(\Theta,\dot{\Theta})\Gamma - \mathbf{C}(\Theta,\upsilon)\Gamma + \mathbf{C}(\Theta,\upsilon)\upsilon \tag{9}$$

$$\mathbf{H}(\Theta)\mathbf{A}(\tilde{\Theta})\dot{\tilde{\Theta}} = \mathbf{H}(\Theta)\mathbf{A}(\tilde{\Theta})\{\Gamma - \lambda\,\mathrm{Tanh}(\tilde{\Theta})\} \tag{10}$$

where, $\upsilon = \dot{\Theta}_d + \lambda\,\mathrm{Tanh}(\tilde{\Theta})$.

Based on the controller defined in Eq. (2), the stability analysis of the robot manipulator proceeds as follows:

Case 1. $\|\Gamma\| > \delta$: In this case, Eq. (8) becomes:

$$\dot{V}_1 = 0.5\,\Gamma^\mathrm{T}\dot{\mathbf{H}}(\Theta)\Gamma + \Gamma^\mathrm{T}\Big\{\mathbf{C}(\Theta,\dot{\Theta})\dot{\Theta} + \chi(\Theta) + \tau_\mathrm{d} - \alpha\,\Gamma - \gamma\,\mathrm{Sgn}(\Gamma) + \mathbf{H}(\Theta)\ddot{\Theta}_\mathrm{d} + \mathbf{H}(\Theta)\,\mathbf{A}(\tilde{\Theta})\dot{\tilde{\Theta}}\Big\}$$

By using Eqs. (9), (10) and property P4, $\dot{V}_1$ is reduced to:

$$\dot{V}_1 = -\Gamma^\mathrm{T}\{\alpha - \mathbf{C}(\Theta,\upsilon) - \mathbf{H}(\Theta)\mathbf{A}(\tilde{\Theta})\}\Gamma - \Gamma^\mathrm{T}\{\gamma\,\mathrm{Sgn}(\Gamma) - \mathbf{C}(\Theta,\upsilon)\upsilon - \mathbf{H}(\Theta)\ddot{\Theta}_\mathrm{d} - \lambda\,\mathbf{H}(\Theta)\mathbf{A}(\tilde{\Theta})\mathrm{Tanh}(\tilde{\Theta}) - \chi(\Theta) - \tau_\mathrm{d}\}$$

Using properties P1, P2, P5 and Eq. (5), $\dot{V}_1$ becomes:

$$\dot{V}_1 \leq -\{\alpha - k_c\left(\|\dot{\Theta}_\mathrm{d}\| + \lambda\sqrt{n}\right) - \lambda_M\{\mathbf{H}\}\}\|\Gamma\|^2 - \Big\{\gamma - k_c\left(\|\dot{\Theta}_\mathrm{d}\| + \lambda\sqrt{n}\right)^2 - \lambda_M\{\mathbf{H}\}\|\ddot{\Theta}_\mathrm{d}\| - \lambda\,\lambda_M\{\mathbf{H}\}\sqrt{n} - k_v - d\Big\}\|\Gamma\|$$

Define the following constants:

$$\zeta_1 = \sup_t\left(\left\|\dot{\Theta}_d\right\|\right), \quad \zeta_2 = \sup_t\left(\left\|\ddot{\Theta}_d\right\|\right) \tag{11}$$

$$\rho = k_c\left(\zeta_1 + \sqrt{n}\lambda\right)^2 + \lambda_M\{\mathbf{H}\}\left(\lambda\sqrt{n} + \zeta_2\right) + k_v + d \tag{12}$$

Then, we have:

$$\dot{V}_1 \le -\left\{\alpha - k_c\left(\lambda\sqrt{n} + \zeta_1\right) - \lambda_M\{\mathbf{H}\}\right\}\|\Gamma\|^2 - \{\gamma - \rho\}\|\Gamma\| \tag{13}$$

Assumption 1: The gain γ is assumed to satisfy:

$$\gamma > max\left\{\left[\delta k_c\left(\lambda\sqrt{n} + \zeta_1\right) + \delta\lambda_M\{\mathbf{H}\}\right], [\rho]\right\} \tag{14}$$

Assumption 2: The gain α is assumed to satisfy:

$$\alpha > k_c\left(\lambda\sqrt{n} + \zeta_1\right) + \lambda_M\{\mathbf{H}\} \tag{15}$$

Then, by using Assumptions 1, 2 and Eq. (7), $\dot{V}_1$ (Eq. (13)) is negative definite and can be further reduced to:

$$\dot{V}_1 \le -\{\gamma - \rho\}\|\Gamma\| \le -\left(\frac{\gamma - \rho}{\sqrt{0.5\,\lambda_M\{\mathbf{H}\}}}\right)V_1^{1/2} \tag{16}$$

From Eq. (16), it can be concluded that Γ approaches the boundary of the set defined by $\|\Gamma\| \le \delta$ (the boundary layer) in finite time. This result is well-established in sliding mode control theory.

Case 2. $\|\Gamma\| \le \delta$: In this case Eq. (8) becomes:

$$\dot{V}_1 = \frac{1}{2}\Gamma^T\dot{\mathbf{H}}(\Theta)\Gamma + \Gamma^T\left\{\mathbf{C}\left(\Theta,\dot{\Theta}\right)\dot{\Theta} + \chi(\Theta) - \gamma\delta^{-1}\Gamma - \alpha\,\delta^{-1}\|\Gamma\|\Gamma + \mathbf{H}(\Theta)\ddot{\Theta}_d + \mathbf{H}(\Theta)\,\mathbf{A}\left(\widetilde{\Theta}\right)\dot{\widetilde{\Theta}} + \tau_d\right\} \tag{17}$$

By using Eqs. (9), (10) and property P4, $\dot{V}_1$ becomes:

$$\dot{V}_1 = -\Gamma^T\left\{\gamma\delta^{-1} - \mathbf{C}(\Theta,\upsilon) - \mathbf{H}(\Theta)\mathbf{A}\left(\widetilde{\Theta}\right)\right\}\Gamma - \alpha\delta^{-1}\|\Gamma\|\Gamma^T\Gamma + \Gamma^T\left\{\mathbf{C}(\Theta,\upsilon)\upsilon + \mathbf{H}(\Theta)\ddot{\Theta}_d - \lambda\,\mathbf{H}(\Theta)\mathbf{A}\left(\widetilde{\Theta}\right)\mathrm{Tanh}\left(\widetilde{\Theta}\right) + \chi(\Theta) + \tau_d\right\} \tag{18}$$

By using P1, P2, P5 and Eq. (5), equation (18) can be simplified to:

$$\dot{V}_1 \le -\kappa\,\|\Gamma\|^2 - \alpha\delta^{-1}\|\Gamma\|^3 + \rho\|\Gamma\|$$

$$\le -(\alpha\delta^{-1}\|\Gamma\|^3 + \xi\kappa\|\Gamma\|^2 - \rho\|\Gamma\|) - (1-\xi)\kappa\|\Gamma\|^2 \tag{19}$$

where $0 < \xi < 1$ and κ is defined by:

$$\kappa = \gamma\delta^{-1} - k_c\left(\lambda\sqrt{n} + \zeta_1\right) - \lambda_M\{\mathbf{H}\} \tag{20}$$

Note: *By multiplying both sides of Eq. (14), which defines Assumption 1, by* $\delta^{-1} > 0$, *we conclude that:* $\gamma\delta^{-1} > max\left\{\left[k_c\left(\lambda\sqrt{n} + \zeta_1\right) + \lambda_M\{\mathbf{H}\}\right], [\delta^{-1}\rho]\right\}$ *Therefore, from Eq. (20), we verify that* $\kappa > 0$.

In the present case, the stability of the variable Γ can be determined from Eq. (19). Specifically, if $\|\Gamma\| \ge \mu$, where:

$$\mu = \rho\,\xi^{-1}\kappa^{-1} \tag{21}$$

then the first term in Eq. (19) will always be less than or equal to zero, and consequently, we can rewrite $\dot{V}_1$ as follows:

$$\dot{V}_1 \le -(1-\xi)\kappa\|\Gamma\|^2 \quad \forall\,\|\Gamma\| \ge \mu \tag{22}$$

Note: *Eq. (21) is derived by manipulating the first term in Eq. (19), specifically by considering the inequality* $(\alpha\delta^{-1}\|\Gamma\|^3 + \xi\,\kappa\,\|\Gamma\|^2 - \rho\|\Gamma\| \ge 0)$ *along with the condition that* $\|\Gamma\| \le \delta$ with $\delta < 1$ *as defined earlier.*

The structures of Eqs. (6) and (22) permit the application of Theorem 4.18 from [25] (see Appendix A). Consequently, we conclude that the closed-loop dynamic system, as defined by Eqs. (1) and (2), is globally uniformly ultimately bounded (GUUB) stable. Therefore, we have $\|\Gamma\| \le \bar{s}$, where the ultimate bound $\bar{s}$ is given by:

$$\bar{s} = \mu\sqrt{\frac{\lambda_M\{\mathbf{H}\}}{\lambda_m\{\mathbf{H}\}}} \tag{23}$$

The stability result given above indicates that the filtered tracking variable, Γ, is GUUB stable. However, we are particularly concerned with the responses of the position and the velocity tracking errors. From Eq. (3), we can determine the upper bound of $\widetilde{\Theta}$. To find this bound, we proceed as follows: Consider the following Lyapunov function:

$$V_2 = \frac{1}{2}\widetilde{\Theta}^T\widetilde{\Theta} \tag{24}$$

The time derivative of V_2 along the trajectories of the dynamic system defined by Eq. (3) is given by:

$$\dot{V}_2 = \widetilde{\Theta}^T\left(-\lambda\,\mathrm{Tanh}\left(\widetilde{\Theta}\right) + \Gamma\right) \le -\lambda\left\|\widetilde{\Theta}\right\|\left\|\mathrm{Tanh}\left(\widetilde{\Theta}\right)\right\| + \bar{s}\left\|\widetilde{\Theta}\right\|$$

$$\le -(1-\xi)\,\lambda\left\|\widetilde{\Theta}\right\|\left\|\mathrm{Tanh}\left(\widetilde{\Theta}\right)\right\| + \left\|\widetilde{\Theta}\right\|\left(\bar{s} - \xi\,\lambda\left\|\mathrm{Tanh}\left(\widetilde{\Theta}\right)\right\|\right) \tag{25}$$

From the last equation, we can conclude that if:

$$\left\|\tilde{\Theta}\right\| \geq \bar{s}\,\lambda^{-1}\xi^{-1} \tag{26}$$

then the second term in Eq. (25) will always be less than or equal to zero. Consequently, $\dot{V}_2$ is negative definite, and can be rewritten as follows:

$$\dot{V}_2 \leq -(1-\xi)\lambda\left\|\tilde{\Theta}\right\|\left\|\mathrm{Tanh}(\tilde{\Theta})\right\| \;\forall\; \left\|\tilde{\Theta}\right\| \geq \bar{s}\,\lambda^{-1}\xi^{-1} \tag{27}$$

Note: *Eq. (26) is derived by manipulating the second term in Eq. (25), specifically by considering the inequality* $\left(\bar{s} - \xi\,\lambda\left\|\mathrm{Tanh}(\tilde{\Theta})\right\| \leq 0\right)$ *along with the fact that* $\left\|\mathrm{Tanh}(\tilde{\Theta})\right\| \leq \left\|\tilde{\Theta}\right\|$.

The structures of Eqs. (24) and (27) allow the application of Theorem 4.18 in [25] to conclude the GUUB stability of the system defined by Eq. (3). In addition, we have $\left\|\tilde{\Theta}\right\| \leq \bar{e}$. The ultimate bound of the position tracking error $\bar{e}$ is calculated as:

$$\bar{e} = \sqrt{\frac{0.5(\lambda^{-1}\xi^{-1}\bar{s})^2}{0.5}} = \frac{\mu}{\lambda\xi}\sqrt{\frac{\lambda_M\{\mathbf{H}\}}{\lambda_m\{\mathbf{H}\}}} \tag{28}$$

From Eq. (3), the upper bound of the velocity tracking error $\dot{\tilde{\Theta}}$ is given by:

$$\left\|\dot{\tilde{\Theta}}\right\| \leq \|\Gamma\| \leq \bar{s} = \mu\sqrt{\frac{\lambda_M\{\mathbf{H}\}}{\lambda_m\{\mathbf{H}\}}} \triangleq \bar{b} \tag{29}$$

From Eqs. (28) and (29), we observe that the ultimate bounds of both the position and velocity tracking errors can be minimized by reducing μ. As shown in Eq. (21), μ can be decreased arbitrarily by increasing κ, which, according to Eq. (20), can be achieved by increasing γ while reducing δ. However, there are limitations to decreasing δ due to the risk of chattering. Similarly, excessively increasing in γ may result in high control activity, potentially causing actuator saturation since γ is active both inside and outside the boundary layer.

To improve controller performance, the following section presents a new method for reducing the ultimate bounds of the tracking variables, while accounting for the restrictions on the values of γ and the boundary layer width δ.

4. A Framework for Enhancing Controller Performance

Before introducing the enhanced controller, it is important to clarify that the restriction on increasing the gain γ, as indicated at the end of the previous section, applies only outside the boundary layer, where the signum vector function is active. However, inside the boundary layer, this vector function is replaced with $\delta^{-1}\Gamma$, where the value of the tracking variable Γ is very small ($\|\Gamma\| \leq \delta$). Given this, we can increase the gain γ only within the boundary layer as needed to reduce the various tracking bounds. To achieve this, we introduce the following nonnegative real-valued function:

$$\psi(\Omega) = \begin{cases} \beta - \gamma & \forall\, \|\Omega\| \leq \delta,\ \Omega \in \mathbb{R}^n \\ 0 & \text{otherwise} \end{cases} \tag{30}$$

Note: *Here, the gain* β *is a large positive constant, significantly greater than* γ ($\beta \gg \gamma$).

The enhanced controller is now defined by:

$$\tau = (\alpha\|\Gamma\| + \psi(\Gamma) + \gamma)\,\mathrm{Sat}(\Gamma) \triangleq \tau_n \tag{31}$$

Note: *The sliding surface* Γ *remain unchanged and is still governed by Eq. (3).*

4.1. Performance and stability analysis of the enhanced control strategy

To analyse the stability of the enhanced control law, we use the same Lyapunov function as in Eq. (6). Now, we consider two cases:

Case I. $\|\Gamma\| > \delta$: In this case, Eq. (31) simplifies to the same structure as Eq. (2) outside the boundary layer. Therefore, the same conclusion derived from Eq. (16) holds.

Case II. $\|\Gamma\| \leq \delta$: Here, Eq. (31) simplifies to:

$$\tau_n = (\alpha\|\Gamma\| + \beta)\delta^{-1}\Gamma \tag{32}$$

Using this modified control law, Eq. (19) transforms into the following format:

$$\dot{V}_1 \leq -(\alpha\delta^{-1}\|\Gamma\|^3 + \xi\kappa_n\|\Gamma\|^2 - \rho\|\Gamma\|) - (1-\xi)\kappa_n\|\Gamma\|^2 \tag{33}$$

where κ_n is the new value of κ, which is defined as:

$$\kappa_n = \beta\delta^{-1} - k_c\left(\lambda\sqrt{n} + \zeta_1\right) - \lambda_M\{\mathbf{H}\} \tag{34}$$

Note: *By comparing Eq. (20) with Eq. (34) and noting that* $\beta \gg \gamma$, *we conclude that* $\kappa_n \gg \kappa$.

The impact of the enhanced control strategy becomes evident when comparing κ_n with κ. The new gain adjustment in Eq. (33) results in the following new value of μ:

$$\mu_n = \rho\, \xi^{-1}\kappa_n^{-1} \tag{35}$$

According to this equation, large values of κ_n cause the new ultimate bound μ_n to approach nearly zero. By comparing Eq. (21) and Eq. (35), and since $\kappa_n \gg \kappa$, we have $\mu_n \ll \mu$. This means that the ultimate bound of the tracking variable Γ is greatly reduced, as expected, by using the enhanced control law defined by Eq. (31).

Following the same analysis as in the previous section, we obtain the following new ultimate bounds:

$$\|\Gamma\| \le \mu_n \sqrt{\frac{\lambda_M\{\mathbf{H}\}}{\lambda_m\{\mathbf{H}\}}} \triangleq \bar{s}_n \tag{36}$$

$$\left\|\tilde{\Theta}\right\| \le \frac{\mu_n}{\lambda\xi}\sqrt{\frac{\lambda_M\{\mathbf{H}\}}{\lambda_m\{\mathbf{H}\}}} \triangleq \bar{e}_n \tag{37}$$

$$\left\|\dot{\tilde{\Theta}}\right\| \le \mu_n \sqrt{\frac{\lambda_M\{\mathbf{H}\}}{\lambda_m\{\mathbf{H}\}}} \triangleq \bar{b}_n \tag{38}$$

The presence of μ_n in place of μ in the above bounds demonstrates that the controller's performance has been significantly improved. This is true because μ_n is considerably smaller—nearly zero—indicating a substantial enhancement in control precision.

5. Enhanced Controller Design Using a Nonlinear PI Sliding Surface

In this section, the performance of the enhanced controller (Eq. (31)) is further improved by introducing a novel nonlinear proportional-integral (PI) sliding surface. The integral term provides the advantage of eliminating steady-state tracking error. The newly proposed sliding surface σ is defined as follows:

$$\sigma = \Gamma + \eta\, \mathrm{Tanh}(\vartheta) \tag{39}$$

$$\dot{\vartheta} = \mathrm{Tanh}(\Gamma\, \delta_1^{-1}) \tag{40}$$

where $\eta > 0$ is a constant gain, and $\delta_1 < 1$ is a small constant.

On the sliding mode ($\sigma = 0$), the system dynamics defined by Eqs. (39) and (40) become:

$$\Gamma = -\eta\, \mathrm{Tanh}(\vartheta) \tag{41}$$

$$\dot{\vartheta} = -\mathrm{Tanh}\left(\delta_1^{-1}\eta\, \mathrm{Tanh}(\vartheta)\right) \tag{42}$$

By pre-multiplying both sides of the last equation by ϑ^{T}, we can demonstrate that Eq. (42) represents a globally asymptotically stable differential equation. Consequently, $\vartheta \to 0$ as $\mathrm{t} \to \infty$. From Eq. (41), it then follows that $\Gamma \to 0$ as $\mathrm{t} \to \infty$. Given the definition of Γ, we conclude that $\tilde{\Theta} \to 0$ as $\mathrm{t} \to \infty$.

The enhanced controller with the PI sliding surface now takes the following form:

$$\tau = \left(\hat{\alpha}\|\sigma\| + \hat{\psi}(\sigma) + \hat{\gamma}\right)\mathrm{Sat}(\sigma) \triangleq \hat{\tau}_{\mathrm{n}} \tag{43}$$

where,

$$\hat{\psi}(\sigma) = \begin{cases} \hat{\beta} - \hat{\gamma} & \forall\, \|\sigma\| \le \delta, \sigma \in \mathbb{R}^n \\ 0 & \text{otherwise} \end{cases} \tag{44}$$

Here, $\hat{\alpha}, \hat{\beta}$, and $\hat{\gamma}$ are the new values of the gains α, β, and γ, with the assumption that $\hat{\beta} \gg \hat{\gamma}$.

Note: *While the thickness of the boundary layer of the new sliding manifold σ can be chosen arbitrarily, it has been selected as δ. This choice does not result in any loss of generality.*

5.1. Stability analysis and performance evaluation of the enhanced controller design with the nonlinear PI sliding surface

The stability analysis of the new dynamic system, as described by Eqs. (1) and (43), is performed by considering the following Lyapunov function:

$$V_3(\sigma) = \tfrac{1}{2}\,\sigma^{\mathrm{T}}\mathbf{H}(\Theta)\sigma \tag{45}$$

Using property P1, we have:

$$\tfrac{1}{2}\lambda_m\{\mathbf{H}\}\|\sigma\|^2 \le V_3(\sigma) \le \tfrac{1}{2}\lambda_M\{\mathbf{H}\}\|\sigma\|^2 \tag{46}$$

The time-derivative of V_3 along the trajectories of the dynamic system defined by Eqs. (1) and (43) is given by:

$$\begin{aligned}\dot{V}_3 = \tfrac{1}{2}\sigma^{\mathrm{T}}\dot{\mathbf{H}}(\Theta)\sigma + \sigma^{\mathrm{T}}\Big\{&\mathbf{C}\big(\Theta,\dot{\Theta}\big)\dot{\Theta} + \chi(\Theta) - \hat{\tau}_{\mathrm{n}} + \tau_{\mathrm{d}} \\ &+ \mathbf{H}(\Theta)\ddot{\Theta}_{\mathrm{d}} + \lambda\,\mathbf{H}(\Theta)\mathbf{A}\big(\tilde{\Theta}\big)\dot{\tilde{\Theta}} \\ &+ \eta\,\mathbf{H}(\Theta)\mathbf{A}(\vartheta)\,\mathrm{Tanh}(\Gamma\,\delta_1^{-1})\Big\}\end{aligned} \tag{47}$$

Using P3, P4, Eq. (3) and Eq. (39), we obtain:

$$\begin{aligned}\dot{V}_3 = \sigma^{\mathrm{T}}\big\{&\mathbf{C}(\Theta,\upsilon_1)\upsilon_1 - \mathbf{C}(\Theta,\upsilon_1)\sigma + \chi(\Theta) - \hat{\tau}_{\mathrm{n}} + \tau_{\mathrm{d}} \\ &+ \mathbf{H}(\Theta)\ddot{\Theta}_{\mathrm{d}} + \lambda\,\mathbf{H}(\Theta)\mathbf{A}\big(\tilde{\Theta}\big)\sigma \\ &- \eta\,\lambda\,\mathbf{H}(\Theta)\mathbf{A}\big(\tilde{\Theta}\big)\,\mathrm{Tanh}(\vartheta) \\ &- \lambda^2\,\mathbf{H}(\Theta)\mathbf{A}\big(\tilde{\Theta}\big)\mathrm{Tanh}\big(\tilde{\Theta}\big) \\ &+ \eta\,\mathbf{H}(\Theta)\mathbf{A}(\vartheta)\mathrm{Tanh}(\Gamma\,\delta_1^{-1})\big\}\end{aligned} \tag{48}$$

where $\upsilon_1 = \upsilon + \eta\ \mathrm{Tanh}(\vartheta)$.

By employing P1, P2, P5 and Eq. (5), $\dot{V}_3$ is upper bounded as follows:

$$\dot{V}_3 \leq -\sigma^{\mathrm{T}}\hat{\tau}_{\mathrm{n}} + \varrho_1\|\sigma\|^2 + \varrho_2\|\sigma\| \tag{49}$$

where ϱ_1 and ϱ_2 are defined by:

$$\varrho_1 = k_c\left[\zeta_1 + \sqrt{n}(\lambda + \eta)\right] + \lambda\,\lambda_M\{\mathbf{H}\} \tag{50}$$

$$\varrho_2 = k_c\left[\zeta_1 + \sqrt{n}(\lambda + \eta)\right]^2 + k_v + \lambda_M\{\mathbf{H}\}\zeta_2 + d + \lambda_M\{\mathbf{H}\}(\eta + \eta\lambda + \lambda^2)\sqrt{n} \tag{51}$$

Assumption 3: It is assumed that:

$$\hat{\alpha} > \varrho_1 \quad \text{and} \quad \hat{\gamma} > max\{\delta\varrho_1, \varrho_2\} \tag{52}$$

Now, the stability of the current system will be analysed as follows:

- $\|\sigma\| > \delta$: In this case, Eq. (49) takes the following form:

$$\dot{V}_3 \leq -(\hat{\alpha} - \varrho_1)\|\sigma\|^2 - (\hat{\gamma} - \varrho_2)\|\sigma\|$$

By Assumption 3, $\dot{V}_3$ is negative definite. Furthermore, using Eq. (46), it can be further reduced as follows:

$$\dot{V}_3 \leq -(\hat{\gamma} - \varrho_2)\|\sigma\| \leq -\left(\frac{\hat{\gamma}-\varrho_2}{\sqrt{0.5\lambda_M\{\mathbf{H}\}}}\right)\{V_3\}^{1/2} \tag{53}$$

From Eq. (53), it can be concluded that σ approach the boundary layer in finite time.

- $\|\sigma\| \leq \delta$: In this case, Eq. (49) becomes:

$$\dot{V}_3 \leq -\hat{\alpha}\delta^{-1}\|\sigma\|^3 - \hat{\kappa}_n\|\sigma\|^2 + \varrho_2\|\sigma\|$$

$$\leq -(\hat{\alpha}\delta^{-1}\|\sigma\|^3 + \xi\hat{\kappa}_n\|\sigma\|^2 - \varrho_2\|\sigma\|) - (1-\xi)\hat{\kappa}_n\|\sigma\|^2 \tag{54}$$

where,

$$\hat{\kappa}_n = \hat{\beta}\delta^{-1} - \varrho_1 \tag{55}$$

From Assumption 3, δ is small, and since $\hat{\beta} \gg \hat{\gamma}$, it follows that $\hat{\kappa}_n > 0$. Moreover, since $\hat{\beta}$ is already very large, it follows that $\hat{\kappa}_n \gg 0$. On the other hand, the structure of Eq. (54) is similar to Eq. (33), and therefore the new value of μ_n is given by:

$$\hat{\mu}_n = \varrho_2\,\xi^{-1}\hat{\kappa}_n^{-1} \tag{56}$$

This equation resembles Eq. (35), and we can conclude that $\hat{\mu}_n$ is very small (nearly zero) due to the large values of $\hat{\kappa}_n$. Likewise, as in Eq. (36), we have:

$$\|\sigma\| \leq \hat{\mu}_n\sqrt{\frac{\lambda_M\{\mathbf{H}\}}{\lambda_m\{\mathbf{H}\}}} \triangleq r \tag{57}$$

Remark: Given $\hat{\mu}_{\mathrm{n}} \approx 0$, we can infer that the ultimate bound (r) is approximately 0.

Now, using Eqs. (3), (39), and (57) along with Eq. (5), we obtain:

$$\|\Gamma\| \leq r, \left\|\tilde{\Theta}\right\| \leq r, \left\|\widetilde{\Theta}\right\| \leq \tanh^{-1}(r\,\lambda^{-1}), \left\|\tilde{\vartheta}\right\| \leq \tanh^{-1}(r\,\eta^{-1}) \tag{58}$$

This equation implies that choosing large values for λ and η, especially considering the proximity of r to zero, can lead to high tracking performance and nearly zero ultimate bounds for the other variables.

6. Illustrative Example and Simulations

To demonstrate the effectiveness of the proposed controller and evaluate its performance through simulation, we present a two-degrees-of-freedom (2-DoF) manipulator with revolute joints in this section. While this paper focuses on the simulation of a 2-DoF robot, it is important to note that this system is a common and well-accepted benchmark in control systems research. The 2-DoF system was chosen because it provides sufficient complexity to validate the effectiveness of the proposed controller.

The components of the robot's inertia matrix are defined as follows [20]:

$$\mathbf{H}_{11} = (m_1 + m_2)L_1^2 + m_2L_2^2 + 2m_2L_1L_2\cos(\theta_2)$$
$$\mathbf{H}_{22} = m_2L_2^2$$
$$\mathbf{H}_{12} = \mathbf{H}_{21} = m_2L_2^2 + m_2L_1L_2\cos(\theta_2)$$

The entries of the Coriolis matrix $\mathbf{C}(\Theta, \dot{\Theta})$ are [20]:

$$\mathbf{C}_{11} = -m_2L_1L_2\,\dot{\theta}_2\sin(\theta_2)$$
$$\mathbf{C}_{12} = -m_2L_1L_2\left(\dot{\theta}_1 + \dot{\theta}_2\right)\sin(\theta_2)$$
$$\mathbf{C}_{21} = m_2L_1L_2\,\dot{\theta}_1\sin(\theta_2)$$
$$\mathbf{C}_{22} = 0$$

If g denotes the acceleration due to gravity, the components of the gravity force vector can be written as [20]:

$$\chi_1 = \mathrm{g}(m_1 + m_2)L_1\cos(\theta_1) + \mathrm{g}\,m_2L_2\cos(\theta_1 + \theta_2)$$
$$\chi_2 = \mathrm{g}m_2L_2\cos(\theta_1 + \theta_2)$$

Here, we assume that $L_1 = L_2 = 1\,(\mathrm{m})$ and $m_1 = m_2 = 1\,(\mathrm{Kg})$.

6.1. Simulations

For the simulations, the desired position trajectories of the links were selected as follows [21]:

$$\theta_{1_d}(t) = -1.9\sin(t) + \sin(2t) + \pi/2$$
$$\theta_{2_d}(t) = -1.9\cos(t) + \cos(2t) + \pi/2$$

The initial conditions of the links are set as $\theta_1(0) = 1\,(\mathrm{rad})$, $\theta_2(0) = 1.5\,(\mathrm{rad})$, $\dot{\theta}_1(0) = 0$ and $\dot{\theta}_2(0) = 0$. The applied external disturbances are time-varying and selected as follows [21]:

$$\tau_{d_1}(t) = 0.5\sin(200\pi t) + 2\sin(t)$$

$$\tau_{d_2}(t) = 0.5\sin(200\pi t) + \cos(2t)$$

These disturbances include terms that simulate high-frequency measurement noise. The design parameters of the controllers for this task are chosen as follows: $\alpha = 12$, $\beta = 650$, $\gamma = 150$, $\hat{\alpha} = 20$, $\hat{\beta} = 500$, $\hat{\gamma} = 200$, $\lambda = 2$, $\eta = 1$, $\delta_1 = 0.01$, and $\delta = 0.1$. These gain values are selected arbitrarily but in accordance with the stability conditions and Assumptions 1-3.

Upon applying the control laws from Eqs. (2), (31) and (43), the simulation results, showing the motion tracking errors and the torque signals for each robot link, are presented in Figures 1–6. The results demonstrate that the controllers perform well in tracking the desired signals despite the presence of disturbances. Additionally, the performance of the three controllers remains similar throughout the simulation time, making it difficult to determine which controller performs best. This was expected, as the behaviour of the controllers differs primarily within the boundary layer zone of the sliding surface. To evaluate the differences in performance more precisely, especially within this boundary layer, we will further analyse the tracking errors in the next subsection.

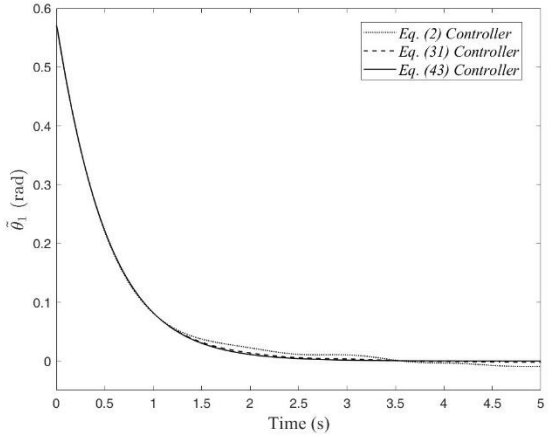

Fig. 1. Position tracking error of the 1st link for all controllers.

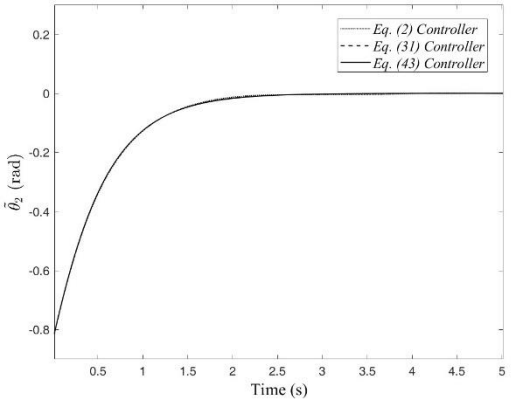

Fig. 2. Position tracking error of the 2nd link for all controllers.

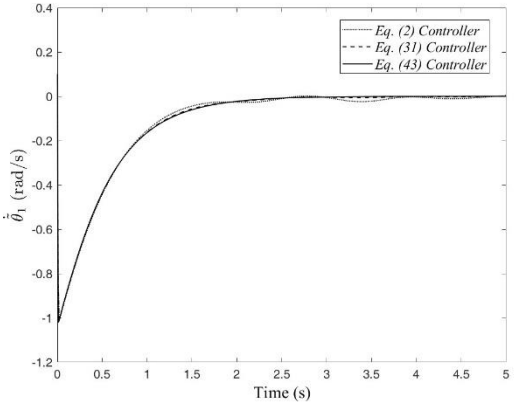

Fig. 3. Velocity tracking error of the 1st link for all controllers.

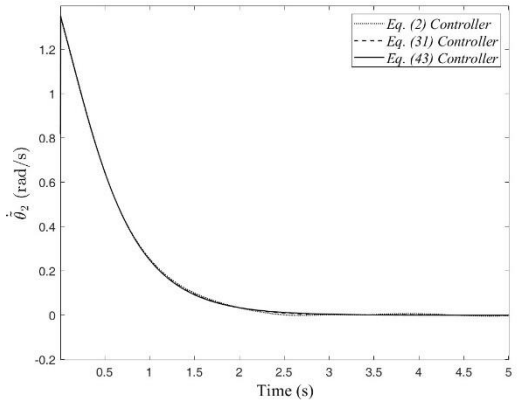

Fig. 4. Velocity tracking error of the 2nd link for all controllers.

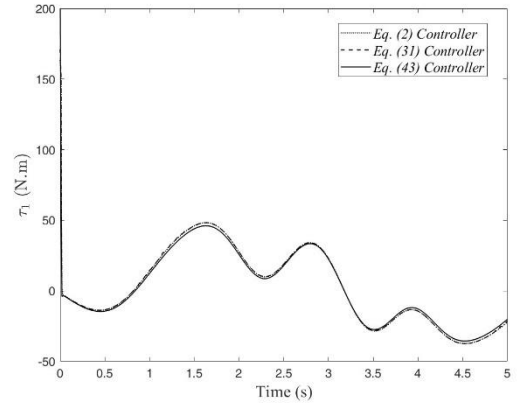

Fig. 5. Control torque of the 1st link for all controllers.

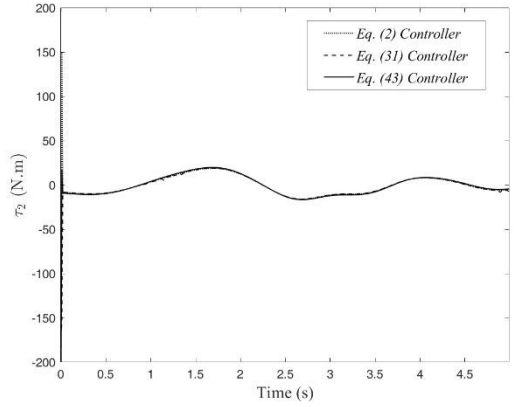

Fig. 6. Control torque of the 2nd link for all controllers.

6.2. Micro analysis of the tracking performance of all controllers

In this subsection, we analyse the tracking performance of all controllers around the zero-error line, focusing on the boundary layer area. The objective is to determine which controller minimizes the tracking errors most effectively within this region. For this analysis, the time period from t=3 (s) to t=15 (s) is selected, as the tracking errors for all controllers converge close to the zero-error line after t=3 (s) (as seen in Figures 1–4). The same simulation setup is used for this comparison, but with an extended simulation time. The results are shown in Figures 7–10. The results reveal that the enhanced controller (Eq. 31) and its modified version (Eq. 43) are the most effective in reducing the tracking errors within the boundary layer. These outcomes are consistent with the theoretical predictions from previous sections. Notably, controller (Eq. 43) outperforms controller (Eq. 31), exhibiting nearly zero tracking errors due to the use of the designed integrator. Consequently, we conclude that controller (Eq. 43) is the best choice among all the evaluated controllers.

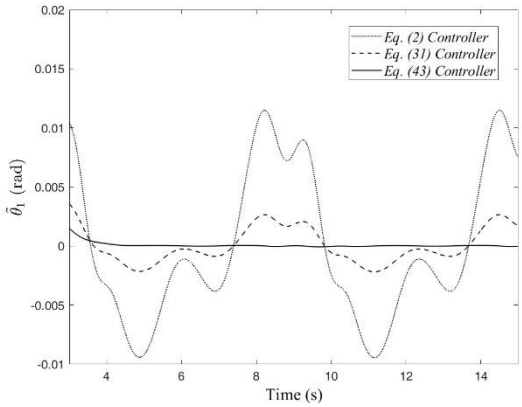

Fig. 7. Position tracking error of the 1st link for all controllers.

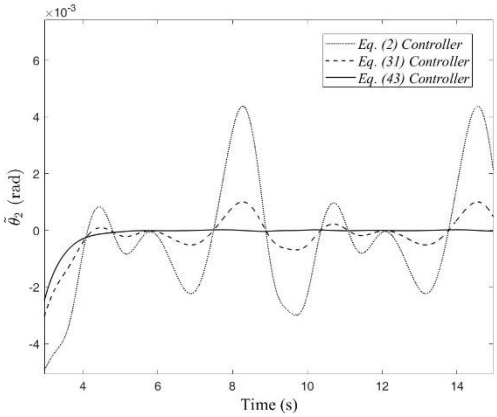

Fig. 8. Position tracking error of the 2nd link for all controllers.

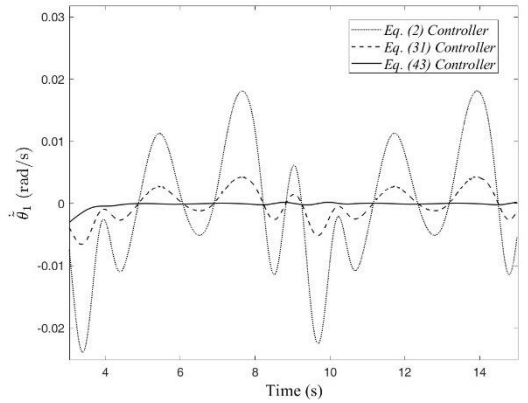

Fig. 9. Velocity tracking error of the 1st link for all controllers.

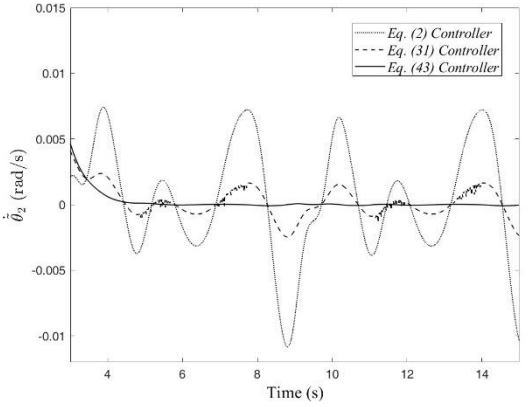

Fig. 10. Velocity tracking error of the 2nd link for all controllers.

7. Conclusion

This study introduces a novel, high-performance continuous sliding mode control (SMC) law for robotic arms. The controller stands out for its structural simplicity and computational efficiency, as it does not rely on the robot's dynamic model. The proposed method guarantees Global Ultimate Bounded (GUB) stability, with calculated ultimate bounds for various tracking errors. To further enhance performance, particularly by minimizing these error bounds, a nonlinear function is incorporated to improve tracking within the boundary layer. This modification increases control effort within the boundary layer, effectively reducing ultimate tracking error bounds. A comprehensive analysis confirms both GUB stability and the effectiveness of this enhanced control strategy. Additionally, replacing the original sliding surface with a proportional-integral (PI) sliding surface further improves performance. The PI-based sliding mode controller maintains GUB stability while achieving superior tracking accuracy. This improvement is evidenced by the near-zero ultimate error bounds across various tracking metrics.

Simulation results from a two-degree-of-freedom robotic manipulator validate the enhanced controller's superiority over the conventional SMC, particularly within the boundary layer, where tracking errors were nearly eliminated. The integrator-enhanced controller consistently delivers high-precision tracking, even in the presence of disturbances, making it a highly effective solution for robotic control applications.

Appendix A

Theorem 4.18 [25]

Let $D \subset \mathbb{R}^n$ be a domain that contains the origin and $V: [0,\infty) \times D \to \mathbb{R}$ be a continuously differentiable function such that

$$\alpha_1(\|x\|) \le V(t,x) \le \alpha_2(\|x\|) \qquad (A.1)$$

$$\frac{\partial V}{\partial t} + \frac{\partial V}{\partial x} f(t,x) \le -W_3(x), \quad \forall \|x\| \ge \mu > 0 \qquad (A.2)$$

$\forall t \ge 0$ and $\forall x \subset D$, where α_1 and α_2 are class $\mathcal{K}$ functions and $W_3(x)$ is a continuous positive definite function. Take $r > 0$ such that $B_r \subset D$ and suppose that

$$\mu < \alpha_2^{-1}\big(\alpha_1(r)\big) \qquad (A.3)$$

Then, there exists a class $\mathcal{KL}$ function β and for every initial state $x(t_0)$, satisfying $\|x(t_0)\| \le \alpha_2^{-1}\big(\alpha_1(r)\big)$, there is $T \ge 0$ (dependent on $x(t_0)$ and μ) such that the solution of ($\dot{x} = f(t,x)$) satisfies

$$\|x(t)\| \le \beta(\|x(t_0), t - t_0\|), \forall\, t_0 \le t \le t_0 + T \qquad (A.4)$$

$$\|x(t)\| \le \alpha_1^{-1}\big(\alpha_2(\mu)\big), \ \forall\, t \ge t_0 + T \qquad (A.5)$$

Moreover, if $D = \mathbb{R}^n$ and α_1 belongs to class $\mathcal{K}_\infty$, then Eq. (A.4) and Eq. (A.5) hold for any initial state $x(t_0)$ with no restriction on how large μ is.

***Note:** Here V is a Lyapunov function and t is the time.*

References

[1] Stepanenko, Y., Cao, Y., and Su, C. Y. “Variable Structure Control of Robotic Manipulator with PID Sliding Surfaces.” International Journal of Robust and Nonlinear Control: IFAC-Affiliated Journal, vol. 8, no. 1, 1998, pp. 79–90.

[2] Ferrara, A., and Magnani, L. “Sliding Mode Motion Control Strategies for Rigid Robot Manipulators.” In Model-Based Reasoning in Science, Technology, and Medicine, pp. 399–412. Springer, 2007.

[3] Hung, J. “Variable Structure Control: A Survey.” IEEE Transactions on Industrial Electronics, vol. 40, 1993, pp. 2–22.

[4] Liu, L., Ding, S., and Yu, X. “Second-Order Sliding Mode Control Design Subject to an Asymmetric Output Constraint.” IEEE Transactions on Circuits and Systems II: Express Briefs, vol. 68, 2021, pp. 1278–1282.

[5] Mei, K., and Ding, S. “High-Order Sliding Mode Controller Design with Asymmetric Output Constraints.” Science China Information Sciences, vol. 65, 2022, pp. 1–2.

[6] Yuan, J., Ding, S., and Mei, K. “Fixed-Time Second-Order Sliding Mode Controller Design with Output Constraint.” Nonlinear Dynamics, vol. 102, 2020, pp. 1567–1583.

[7] Sabanovic, A. “Variable Structure Systems with Sliding Modes in Motion Control: A Survey.” IEEE Transactions on Industrial Informatics, vol. 7, 2011, pp. 212–223.

[8] Khosravi, M., and Taghirad, H. “Dynamic Modeling and Control of Parallel Robots with Elastic Cables: Singular Perturbation Approach.” IEEE Transactions on Robotics, vol. 30, 2014, pp. 694–704.

[9] Zhao, Z., Yang, J., Li, S., Yu, X., and Wang, Z. “Continuous Output Feedback Terminal Sliding Mode Control for Uncertain Systems with a DC–AC Inverter Example.” IEEE Transactions on Circuits and Systems II: Express Briefs, vol. 65, 2017, pp. 71–75.

[10] Slotine, J., and Li, W. Applied Nonlinear Control. Prentice Hall, 1991.

[11] Slotine, J. “Sliding Controller Design for Nonlinear Systems.” International Journal of Control, vol. 40, 1984, pp. 421–434.

[12] Emel’yanov, S., and Korovin, S. “High-Order Sliding Modes in Control Systems.” Computational Mathematics and Mathematical Physics, vol. 7, 1996, pp. 294–318.

[13] Park, K., and Lee, J. “Sliding Mode Controller with Filtered Signal for Robot Manipulators Using Virtual Plant/Controller.” Mechatronics, vol. 7, 1997, pp. 277–286.

[14] Tuan, L., Joo, Y., Duong, P., and Tien, L. “Parameter Estimator Integrated Sliding Mode Control of Dual Arm Robots.” International Journal of Control, Automation and Systems, vol. 15, 2017, pp. 2754–2763.

[15] Cheng, C., Chien, S., and Shih, F. “Design of Robust Adaptive Variable Structure Tracking Controllers with Application to Rigid Robot Manipulators.” IET Control Theory & Applications, vol. 4, 2010, pp. 1655–1664.

[16] Tuan, L., Joo, Y., Tien, L., and Duong, P. “Adaptive Neural Network Second-Order Sliding Mode Control of Dual Arm Robots.” International Journal of Control, Automation and Systems, vol. 15, 2017, pp. 2883–2891.

[17] Yi, S., and Zhai, J. “Adaptive Second-Order Fast Nonsingular Terminal Sliding Mode Control for Robotic Manipulators.” ISA Transactions, vol. 90, 2019, pp. 41–51.

[18] Ji, P., Li, C., and Ma, F. “Sliding Mode Control of Manipulator Based on Improved Reaching Law and Sliding Surface.” Mathematics, vol. 10, no. 11, p. 1935, 2022,

[19] Xian, J., Shen, L., Chen, J., and Feng, W. “Continuous Sliding Mode Control of Robotic Manipulators Based on Time-Varying Disturbance Estimation and Compensation.” IEEE Access, vol. 10, 2022, pp. 43473–43480.

[20] Lewis, F., Abdallah, C., and Dawson, D. Robot Manipulator Control Theory and Practice. Marcel Dekker, 2004.

[21] Yu, S., Yu, X., Shirinzadeh, B., and Man, Z. “Continuous Finite-Time Control for Robotic Manipulators with Terminal Sliding Mode.” Automatica, vol. 41, 2005, pp. 1957–1964.

[22] Ortega, R., Loria, A., Nicklasson, P., and Sira-Ramirez, H. Passivity-Based Control of Euler-Lagrange Systems. Springer-Verlag, 1998.

[23] Kasac, J., Novakovic, B., Majetic, D., and Brezak, D. “Performance Optimization of Saturated PID Controller for Robot Manipulators.” Proceedings of the 10th IEEE International Conference on Methods and Models in Automation and Robotics, Miedzyzdroje, Poland, 2004.

[24] Kelly, R., Santibáñez, V., and Loria, A. Control of Robot Manipulators in Joint Space. Springer-Verlag, 2005.

[25] Khalil, H. Nonlinear Systems. Prentice Hall, 2002.